Remote Sensing of Environment 142 (2014) 111–121

Contents lists available at ScienceDirect

Remote Sensing of Environment

journal homepage: www.elsevier.com/locate/rse

Evaluation of the VIIRS and MODIS LST products in an arid area of Northwest China ☆

Hua Li [a,b], Donglian Sun [b], Yunyue Yu [c], Hongyan Wang [b,d], Yuling Liu [e], Qinhuo Liu [a,*], Yongming Du [a], Heshun Wang [a], Biao Cao [a]

[a] State Key Laboratory of Remote Sensing Science, Institute of Remote Sensing and Digital Earth, Chinese Academy of Sciences, Beijing 100101, China
[b] Department of Geography and Geo-Information Science, George Mason University, Fairfax, VA 22030, USA
[c] NOAA/NESDIS Center for Satellite Application and Research, College Park, MD 20742, USA
[d] Department of Marine Technology, College of Information Science and Engineering, Ocean University of China, Qingdao 266100, China
[e] Earth System Science Interdisciplinary Center, University of Maryland, College Park, MD 20740, USA

ARTICLE INFO

Article history:
Received 16 July 2013
Received in revised form 8 November 2013
Accepted 9 November 2013
Available online 15 December 2013

Keywords:
Evaluation
Land surface temperature
VIIRS
MODIS
HiWATER

ABSTRACT

In this study, the Visible Infrared Imager Radiometer Suite (VIIRS) land surface temperature (LST) environmental data record (EDR) and Moderate Resolution Imaging Spectroradiometer (MODIS) L2 swath LST products (collection 5) from both the Terra and Aqua satellites were evaluated against ground observations in an arid area of northwest China during the Heihe Watershed Allied Telemetry Experimental Research (HiWATER) experiment. Four barren surface sites were chosen for the evaluation, which took place from June 2012 to April 2013. The results show that the current VIIRS LST products demonstrate a reasonable accuracy, with an average bias of 0.36 K and −0.58 K and an average root mean square error (RMSE) of 2.74 K and 1.48 K for the four sites during daytime and nighttime, respectively. The accuracy of the nighttime LST is much better than that of daytime. Furthermore, it was also found that the VIIRS split-window (SW) algorithm provides better performance than the VIIRS dual split-window (DSW) algorithm during both daytime and nighttime. For MODIS LST products, the results show that both Terra and Aqua MODIS C5 LST products underestimate the LST for the four barren surface sites at daytime, and the biases and RMSEs are much larger for Aqua, with biases varies from −0.91 K to −3.13 K for Terra and from −1.31 K to −3.76 K for Aqua.

1. Introduction

Land surface temperature (LST) is a key parameter for hydrological, meteorological, climatological and environmental studies because it combines the results of all surface–atmosphere interactions and energy fluxes between the atmosphere and the surface (Anderson, Norman, Diak, Kustas, & Mecikalski, 1997; Anderson et al., 2011; Wan & Dozier, 1996; Weng, Lu, & Schubring, 2004; Zhou et al., 2003). Remote sensing in the thermal infrared (TIR) provides a unique method of obtaining LST information at the regional and global scales. Many efforts have been devoted to the establishment of methodology for retrieving the LST from remote sensing data and significant progress has been achieved over the past few decades. Many algorithms for LST retrieval have been proposed, including the single-channel algorithm (Jiménez-Muñoz & Sobrino, 2003; Li et al., 2010; Qin, Karnieli, & Berliner, 2001), the spilt-window (SW) algorithm (Sun & Pinker, 2003; Wan & Dozier, 1996; Yu, Privette, & Pinheiro, 2008; Yu et al., 2009) and the temperature emissivity separation (TES) algorithm (Gillespie et al., 1998), among others (Li, Tang et al., 2013). The SW algorithm is the most widely used algorithm for LST retrieval due to its simplicity and robustness. This algorithm corrects for atmospheric effects in the TIR bands using the differential atmospheric absorption in the two adjacent channels centered at 11 μm and 12 μm. Many operational LST products have been generated using different SW algorithms, i.e., the Advanced Very High Resolution Radiometer (AVHRR) (Pinheiro et al., 2007), Advanced Along-Track Scanning Radiometer (AATSR) (Coll et al., 2012), Moderate Resolution Imaging Spectroradiometer (MODIS) (Wan & Dozier, 1996), Spinning Enhanced Visible and Infrared Imager (SEVIRI) (Niclòs, Galve, Valiente, Estrela, & Coll, 2011) and Geostationary Operational Environmental Satellites (GOES) (Sun, Yu, Fang, & Liu, 2013).

The Suomi National Polar-orbiting Partnership (NPP) satellite was launched on October 28, 2011, and the Visible Infrared Imager Radiometer Suite (VIIRS) onboard the NPP satellite provides a majority of the Environmental Data Records (EDRs). One of the key EDRs is the VIIRS LST, which is derived from the VIIRS data using a set of split-window and dual split-window algorithms. The coefficients of the LST algorithm are surface type dependent, in reference to the International

* Corresponding author. Tel.: +86 1064849840.
E-mail address: qhliu@irsa.ac.cn (Q. Liu).

0034-4257/$ – see front matter © 2013 The Authors. Published by Elsevier Inc. All rights reserved.
http://dx.doi.org/10.1016/j.rse.2013.11.014

Geosphere-Biosphere Programme (IGBP) types (Sun, Ji, Ardanuy, Keally, & Yang, 2000; Sun & Pinker, 2003; Yu, Privette, & Pinheiro, 2005).

The LST products from different sensors have been used successfully in many scientific fields, e.g., GOES LST products have been used for evapotranspiration estimation (Anderson et al., 2011), MODIS LST products have been used for air temperature estimation (Vancutsem, Ceccato, Dinku, & Connor, 2010) and urban heat island monitoring (Rajasekar & Weng, 2009). In particular, using the LST products generated from AVHRR, MODIS and VIIRS can aid in the development of long-term moderate-resolution LST climate data records (CDR), and the three basic sensor designs will provide a 50-year continuous data record (Yu et al., 2008).

However, the LST products are not widely used by operational weather and climate centers via direct analysis or data assimilation in land surface and climate models due to the lack of inclusion of detailed uncertainties (Guillevic et al., 2012; Hulley, Hughes, & Hook, 2012). Thus, validations of different LST products are necessary to provide LST users with data quality information, to identify possible deficiencies and to further improve the LST retrieval algorithms (Coll, Wan, & Galve, 2009).

Two methods are commonly applied to validate the LST products generated from remote sensing data: the temperature-based method (T-based) and the radiance-based method (R-based). The T-based method involves direct comparison with ground measurements performed at the thermally homogenous sites concurrent with the satellite overpass. Many dedicated field experiments have been conducted to evaluate the accuracy of different LST products over different surfaces, including lakes and agricultural lands (Coll et al., 2005, 2007; Hook, Vaughan, Tonooka, & Schladow, 2007; Li, Tang, et al., 2013; Wan, 2008; Wan, Zhang, Zhang, & Li, 2002). However, qualified ground LST measurements are still rare. Certain researchers have used surface longwave radiation observations to retrieve the LST for long-term LST product evaluation (Sun & Pinker, 2003; Wang & Liang, 2009; Wang, Liang, & Meyer, 2008; Yu et al., 2009, 2012). In addition, many studies have only used the nighttime observations for evaluation in order to mitigate the scale mismatch issue that occurs between ground point measurements and the satellite pixel scale (Wang & Liang, 2009; Wang et al., 2007, 2008).

The R-based method does not require ground measured LST values but does require atmospheric temperature and water vapor profiles and the surface emissivity over the validation site at the time of satellite overpass (Coll et al., 2009; Wan, 2014; Wan & Li, 2008). The in-situ LST is estimated from the satellite TOA radiance using the surface emissivity of the selected site, nearly concurrent atmospheric profile, and an atmospheric radiative transfer model. The difference between the LST product and the calculated in-situ LST is the accuracy of the satellite LST product. This method was firstly developed for validation of the standard MODIS LST products without the need for rigorous ground measurements. Later, it was successfully applied to the evaluation of AATSR and SEVIRI LST products (Coll et al., 2009, 2012; Niclòs et al., 2011). The R-based method is advantageous for those sensors with coarse spatial resolution and can be applied to any location with small spatial and temporal variations in surface emissivity, such as the AIRS (Hulley & Hook, 2012), which is difficult to apply with the T-based method.

Before the launch of Suomi NPP, the VIIRS LST product algorithm was evaluated using simulated data and MODIS data as a proxy (Yu et al., 2005). After launch, the VIIRS LST EDR requires extensive evaluation to identify its real performance. The objective of this paper is to evaluate the VIIRS LST EDR using ground measurements collected in an arid area of northwest China during the Heihe Watershed Allied Telemetry Experimental Research (HiWATER) experiment (Li, Cheng, et al., 2013). This work is a part of the VIIRS LST evaluation efforts of the JPSS land product calibration and validation plan. Additionally, the MODIS L2 swath LST products (collection 5) from both Terra and Aqua will be evaluated for comparison. More specifically, this paper primarily focuses on T-based method at the barren surface sites where LST validation activities have been relatively rare for this surface type.

The outline of this paper is as follows. Section 2 provides a brief description of the VIIRS and MODIS LST retrieval algorithms. Section 3 gives a detailed description of the ground LST measurements collected in the HiWATER experiment, the satellite data used in this paper, and the ground data processing method. The results of the LST evaluation are presented and analyzed in Section 4. Finally, the discussion and conclusions of this study are summarized in Section 5.

2. VIIRS and MODIS LST retrieval algorithms

2.1. VIIRS LST algorithms

The VIIRS contains 22 spectral bands, which include 16 moderate-resolution (750 m) bands and 5 high-resolution (375 m) imagery bands, plus one panchromatic Day/Night band. The VIIRS LST EDR is based on two kinds of algorithms and is a swath product similar to the MODIS Level 2 swath products (Yu et al., 2005). The baseline is a split window (SW) algorithm that applies data from the VIIRS M15 and M16 bands centered at wavelengths of 10.8 μm and 12.0 μm, respectively (Sun & Pinker, 2003). The optional dual-split window (DSW) algorithm applies additional two shortwave infrared bands M12 and M13 centered at wavelengths of 3.75 μm and 4.0 μm, respectively (Sun et al., 2000). The algorithms are described as follows:SW algorithm:

$$\begin{aligned} \mathrm{LST}_i = {} & c_0(i) + c_1(i)T_{11} + c_2(i)(T_{11} - T_{12}) \\ & + c_3(i)(\sec\theta - 1) + c_4(i)(T_{11} - T_{12})^2. \end{aligned} \tag{1}$$

Daytime DSW algorithm:

$$\begin{aligned} LST_i = {} & a_0(i) + a_1(i)T_{11} + a_2(T_{11} - T_{12}) + a_3(i)(\sec\theta - 1) \\ & + a_4(i)T_{3.75} + a_5(i)T_{4.0} + a_6(i)T_{3.75}\cos\varphi \\ & + a_7(i)T_{4.0}\cos\varphi + a_8(i)(T_{11} - T_{12})^2 \end{aligned} \tag{2}$$

Nighttime DSW algorithm:

$$\begin{aligned} \mathrm{LST}_i = {} & b_0(i) + b_1(i)T_{11} + b_2(T_{11} - T_{12}) + b_3(i)(\sec\theta - 1) \\ & + b_4(i)T_{3.75} + b_5(i)T_{4.0} + b_6(i)T_{3.75}^2 + b_7(i)T_{4.0}^2 \\ & + b_8(i)(T_{11} - T_{12})^2 \end{aligned} \tag{3}$$

where i is the index of 17 IGBP surface types; $a_j(i)$, $b_j(i)$ and $c_j(i)$ are the algorithm regression coefficients in which j represents the term's sequential position in the equation; $T_{3.75}$, $T_{4.0}$, T_{11} and T_{12} are the brightness temperatures of the M12, M13, M15 and M16 VIIRS bands, respectively; θ is the satellite zenith angle, and φ is the solar zenith angle. Note that the DSW algorithm consists of daytime and nighttime versions, and was applied as baseline algorithm before August 10, 2012.

2.2. MODIS LST algorithm

The standard MODIS LST products include one Level 2 swath product and six Level 3 gridded products. These products are generated using two different algorithms: a generalized split window (GSW) algorithm (Wan & Dozier, 1996) and a Day/Night algorithm (Wan & Li, 1997). In this paper, only the MODIS Level 2 swath products (MOD11_L2/MYD11_L2) are used for evaluation. The GSW algorithm is described as follows:

$$\begin{aligned} T_s = {} & C + \left(A_1 + A_2\frac{1-\varepsilon}{\varepsilon} + A_3\frac{\Delta\varepsilon}{\varepsilon^2}\right)\frac{T_{31} + T_{32}}{2} \\ & + \left(B_1 + B_2\frac{1-\varepsilon}{\varepsilon} + B_3\frac{\Delta\varepsilon}{\varepsilon^2}\right)\frac{T_{31} - T_{32}}{2} \end{aligned} \tag{4}$$

with $\varepsilon = (\varepsilon_{31} + \varepsilon_{32}) / 2$ and $\Delta\varepsilon = \varepsilon_{31} - \varepsilon_{32}$, where T_s is the LST, T_{31} and T_{32} are the MODIS bands 31 and 32 brightness temperatures, respectively; ε_{31} and ε_{32} are the MODIS bands 31 and 32 surface emissivities, respectively; and C, A_1, A_2, A_3, B_1, B_2 and B_3 are the algorithm regression coefficients.

3. Experimental data

3.1. HiWATER experiment

HiWATER is an ongoing watershed-scale eco-hydrological experiment designed from an interdisciplinary perspective to address problems that include heterogeneity, scaling, uncertainty and closing of the water cycle at the watershed scale (Li, Cheng, et al., 2013; Liu et al., in preparation). The experiment was performed in the Heihe River Basin, which is in the arid region of northwest China (Gansu province) and the coordinate range is between 97.1°E–102.0°E and 37.7°N–42.7°N. The overall objective of the HiWATER experiment is to improve the observability of hydrological and ecological processes, to build a world-class watershed observing system and to enhance the applicability of remote sensing in integrated eco-hydrological studies and water recourse management at the basin scale (Li, Cheng, et al., 2013). Three key experimental areas (KEAs) were selected in which to conduct intensive and long-term observations: the cold region experimental area in the upper reaches, the artificial oasis experimental area in the middle reaches, and the natural oasis experimental area downstream. Certain foci experiment areas (FEAs) also exist in each KEA, which were designed as hierarchically nested locations of multi-scale ground observations. Detailed information on the HiWATER experiment can be found in Li, Cheng, et al. (2013) and at http://hiwater.westgis.ac.cn/english/. The field observations and remotely sensed data used in this study were derived from the KEA of the middle stream during the period from June 2012 to April 2013.

3.2. Ground site

The LST evaluation in this study uses four sites, and their geographic locations and the descriptions are presented in Fig. 1 and Table 1, respectively. The four sites are located in large flat areas around the oasis. Four sites contain three land surface types, i.e., Gobi (GB), sand dune (SSW) and desert steppe (HZZ, JCHM). Gobi site consists of small gravel, bare soil and small *Alhagi sparsifolia*. *A. sparsifolia* is a spiny, perennial subshrub which mainly grows in salinized and arid regions in the native ranges of northwestern China, Central Asia, India, and Middle and Near East (Gui, Zeng, Liu, & Zhang, 2013). The sand dune site is more uniformly, but sparsely covered by *A. sparsifolia*. The sand dune is approximately 10 to 20 m high and the sand is primarily composed of quartz. Desert steppe site consists of bare soil and *A. sparsifolia*, and the ground cover fraction of *A. sparsifolia* is approximately 0.1. According to the atmospheric profile product from MODIS (MOD07), the total water vapor contents for the study area ranged from 0.5 to 2.6 g/cm^2 from June to September, 2012.

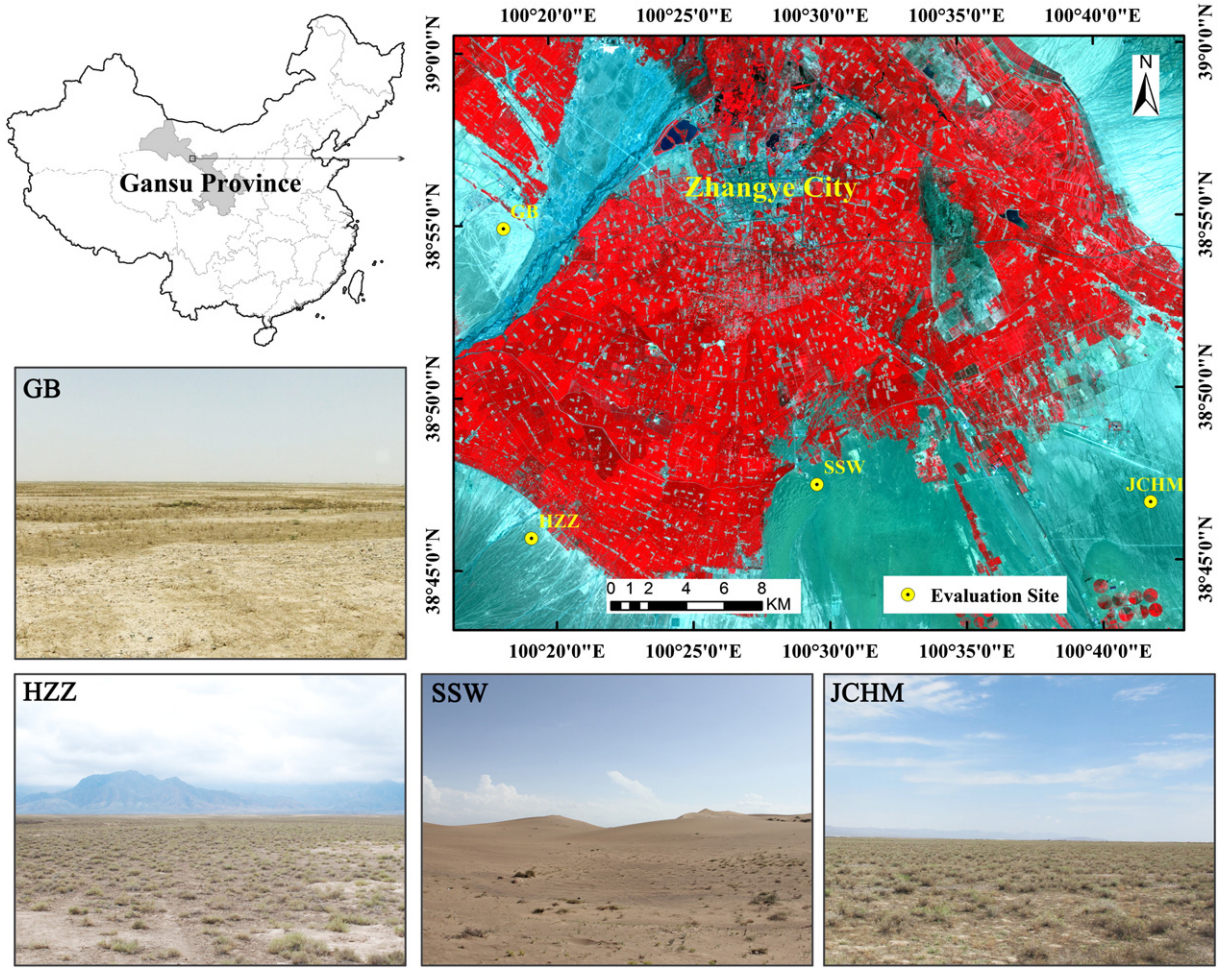

Fig. 1. Spatial distribution and ground photographs of the four barren surface sites in this study. The upper right image is the ASTER L1B VNIR image covering the study area on July 10, 2012. The RGB components are channels 3 (0.81 μm), 2 (0.66 μm) and 1 (0.56 μm), respectively, with 15 m resolution.

Table 1
Descriptions of the four sites.

Site	Latitude Longitude	Elevation (m)	Land cover	VIIRS land cover type	MODIS IGBP land cover type	Instrument	Measurement height (m)	Time period (year/month/day)
GB	38.9150 N 100.3042 E	1567	Gobi	Barren	Barren or sparsely vegetated	CNR1 net radiometers	6	2012/07/22–2012/10/14
SSW	38.7892 N 100.4933 E	1555	Sand dune	Barren	Barren or sparsely vegetated	CNR1 net radiometers	6	2012/06/08–2012/10/14
HZZ	38.7652 N 100.3186 E	1735	Desert steppe	Barren	Grasslands	SI-111 radiometer	2.65	2012/06/04–2012/10/14
JCHM	38.7781 N 100.6967 E	1625	Desert steppe	Barren/Grasslands	Grasslands	SI-111 radiometer	4	2012/06/29–2013/04/23

3.3. Ground instrument

Two types of instruments are equipped in these sites. The GB and SSW sites are each equipped with one Kipp & Zonen CNR1 net radiometers, which observes the surface at nadir from a 6 m height and the HZZ and JCHM sites are equipped with Apogee SI-111 thermal infrared radiometers, which directly measure the land surface temperature. These sites are also equipped with other meteorological instruments to measure the magnitudes of the air temperature, humidity and wind speed (except for the JCHM site). The HZZ site is each equipped with two SI-111 radiometers. Both of the radiometers observe the surface at nadir from heights of 2.65 m to obtain a target footprint of 3.6 m^2 for the HZZ site. Two SI-111 radiometers are used at the JCHM site; one observes the surface at nadir from a 4 m height with a footprint of 8 m^2, and the other views the sky at an effective angle of approximately 55° from the zenith to measure the atmospheric downwelling radiance.

The SI-111 radiometers and CNR1 net radiometers are sampled every 30 s at the GB, SSW and HZZ sites, and the 30-second samples are averaged to obtain 1 minute values. All data are transmitted and archived in the data center using wireless transmission techniques. The sampling frequency of the SI-111 radiometers is 5 s at the JCHM site and the data are archived in a Campbell CR1000 datalogger.

3.4. Ground LST estimation

For the GB and SSW sites, the LST was estimated from the upwelling and downwelling longwave radiation using the following equation:

$$T_s = \left[\frac{F^{\uparrow} - (1-\varepsilon_b)\cdot F^{\downarrow}}{\varepsilon_b \cdot \sigma}\right]^{1/4} \quad (5)$$

where T_s is the LST, $F^{\uparrow}$ is the surface upwelling longwave radiation, ε_b is the surface broadband emissivity (BBE), σ is the Stefan–Boltzmann's constant ($5.67 \times 10^{-8}\ Wm^{-2}\ K^{-4}$), and $F^{\downarrow}$ is the atmospheric downwelling longwave radiation at the surface.

Cheng, Liang, Yao, and Zhang (2013) have indicated that 8–13.5 μm is the optimal broadband emissivity spectral range for representing the entire longwave range. Thus, the BBE for 8–13.5 μm is estimated from the ASTER narrowband emissivities using the following linear equation (Cheng et al., 2013):

$$\varepsilon_b = 0.197 + 0.025\varepsilon_{10} + 0.057\varepsilon_{11} + 0.237\varepsilon_{12} + 0.333\varepsilon_{13} + 0.146\varepsilon_{14} \quad (6)$$

where ε_b is the surface broadband emissivity, and ε_{10}–ε_{14} are the five ASTER narrowband emissivities.

Twelve ASTER images were collected in the experimental area from May to September of 2012. Table 2 presents a list of all dates and the overpass times of the ASTER data. The land surface temperature and emissivities were derived from the ASTER data using the TES algorithm (Gillespie et al., 1998), combined with the Water Vapor Scaling (WVS) atmospheric correction method (Li et al., in preparation; Tonooka, 2005). The average ε_b values of 0.955 ± 0.007 and 0.922 ± 0.005 were calculated from the 12 ASTER scenes for the GB and SSW sites, respectively.

For the HZZ and JCHM sites, the SI-111 radiometer measured radiometric temperatures were corrected for emissivity and the downward sky irradiance effects. Because no atmospheric downwelling radiance measurements were collected at the HZZ site and the distance between HZZ site and JCHM site was close to 30 km, assuming the atmosphere was stable in this distance in the arid area, the atmospheric downwelling radiance measurements from JCHM were used directly for the HZZ site. If T_r is the radiometric temperature measured by a radiometer, the true land surface temperature T_s is given by:

$$B(T_s) = \left[B(T_r) - (1-\varepsilon)L_{sky}\right]/\varepsilon \quad (7)$$

where B is the Planck function weighted for the spectral response function of the SI-111 radiometer, ε is the surface emissivity of SI-111 channel and L_{sky} is the downward sky irradiance divided by π.

The HZZ and JCHM sites exhibit the same land cover types, both consisting of bare soil and *A. sparsifolia*. Thus, the emissivities of the sites were determined using the vegetation cover method (Valor & Caselles, 1996). This method requires the vegetation and background emissivities. During the field experiment, the emissivities of bare soil and *A. sparsifolia* in the JCHM sites were measured using the ABB BOMEM MR304 spectroradiometers and a diffuse golden plate, which were used to obtain the radiometric data of the samples and the corresponding atmospheric downward radiance. The spectral resolution of the MR304 is 1 cm^{-1}. The emissivity spectra in the range of 8–14 μm were retrieved using the Iterative Spectrally Smooth Temperature and

Table 2
List of dates and overpass times of the ASTER data and standard deviation of 11 × 11 ASTER LST pixels at four sites.

Case	Date (month/day/year)	Overpass time (UTC)	STD (K)			
			GB	SSW	HZZ	JCHM
1	05/30/2012	04:19	0.82	1.37	0.58	0.58
2	06/15/2012	04:19	0.87	0.85	0.70	0.42
3	06/24/2012	04:13	0.77	1.03	0.64	0.54
4	07/10/2012	04:13	1.12	1.44	0.81	0.33
5	08/02/2012	04:19	1.35	1.82	0.70	0.52
6	08/11/2012	04:13	1.24	1.48	0.87	0.59
7	08/18/2012	04:19	0.63	0.64	0.78	0.58
8	08/27/2012	04:13	1.04	0.99	0.51	0.56
9	09/03/2012	04:19	1.13	1.08	0.40	0.57
10	09/12/2012	04:13	1.09	1.01	1.07	0.60
11	09/19/2012	04:19	1.11	0.77	0.63	0.41
12	09/28/2012	04:13	1.00	0.86	0.54	0.59
All			1.01	1.11	0.69	0.52

Emissivity Separation (ISSTES) algorithm, which has been proven as an effective algorithm with high accuracy for temperature and emissivity retrieval (Borel, 1998; Ingram & Muse, 2001). Nine and five valid emissivity samples were obtained for bare soil and *A. sparsifolia*, respectively. Thus, the SI-111 channel emissivity values of 0.969 ± 0.002 and 0.980 ± 0.003 were obtained for bare soil and *A. sparsifolia* respectively, at the JCHM site. The Fractional Vegetation Cover (FVC) of the JCHM site was measured using a photographic method (Liu, Mu, Wang, & Yan, 2011) at nadir view, and a value of 0.1 was obtained. Finally, an emissivity value of 0.970 ± 0.002 was obtained for the JCHM site. We also used ground measurements from the JCHM site in winter, and therefore, the snow emissivity is used if the surface type of the VIIRS LST EDR indicates snow. Three snow emissivity samples in the ASTER spectral library were used to calculate the channel emissivity (Baldridge, Hook, Grove & Rivera, 2009), and an average value of 0.984 was obtained. The emissivity measurements were not performed at the HZZ site, but we analyzed the ASTER BBE values of the HZZ and JCHM sites and found that the BBE values of these two sites were nearly the same. Therefore, the emissivity value of the JCHM site was used directly for the HZZ site when retrieving the LST.

3.5. Ground LST uncertainty

The absolute accuracy $\delta(\text{cal})$ of the SI-111 radiometer is ±0.2 K at temperatures from 238 K to 338 K (from factory calibration; http://www.apogeeinstruments.com/infraredradiometer), and these radiometers have been successfully used in many field experiments for LST validation purposes (Li, Liu, Du, Jiang, & Wang, 2013; Niclòs et al., 2011). The CNR1 net radiometers were compared with an Eppley Precision Infrared Radiometer (PIR), which is the World Meteorological Organization (WMO) first-class radiometer during the HiWATER experiments. The differences in the longwave radiation were approximately −8 W m^{-2} to 3 W m^{-2} (Xu et al., 2013), with a small difference at night and a larger difference around noon during the daily course of radiation (8 W m^{-2} at daytime and 3 W m^{-2} at nighttime), equivalent to an error of 1.2 K in the LST at daytime and 0.5 K in the LST at nighttime, respectively.

Considering an emissivity uncertainty of ±0.01 for the ground LST retrieval of each site, which is larger than the uncertainties in the emissivity values listed above, the emissivity correction errors $\delta(\text{emis})$ range from ±0.3 K to ±0.5 K depending on the magnitude of L_{sky} and the temperature range in this study.

The in-situ LSTs were calculated by averaging the ground measurements collected by the radiometers within 3 min centered at the satellite acquisition times over the sites. The standard deviation (STD) of the obtained LSTs was calculated as the temporal variability of the LST at each evaluation sites $\delta(\text{temp})$ and was smaller than 0.25 K for all sites.

The uncertainties associated with the spatial thermal variability of the evaluation sites were analyzed using the twelve ASTER LST products. The LSTs for the 11 × 11 pixels (1 km^2) centered on the evaluation site were extracted and the STD was calculated for each scene. All the STD values of twelve ASTER scenes for four sites are summarized in Table 2. The average STD of twelve ASTER scenes was considered as an estimate of the spatial uncertainties associated with the use of in-situ LSTs to evaluate the satellite LST product due to the spatial dissimilarity problem $\delta(\text{spat})$. Average values of 1.01 K, 1.11 K, 0.68 K and 0.52 K were obtained for the GB, SSW, HZZ and JCHM sties, respectively. Fig. 2 shows histograms of the LST for 11 × 11 pixels for the four sites on August 27, 2012. The STD values of this day were very close to the average values for the four sites. It can be found that the LST differences between about 95% pixels are within 4 K for GB and SSW sites and 2 K for HZZ and JCHM sites. These results indicate that the selected four barren surface sites reveal a relatively high thermal homogeneity in the daytime. Additionally, it should be noted that the $\delta(\text{spat})$ should be smaller at nighttime.

Therefore, the total uncertainty in the temperature measurement for each site $\delta(T_s)$ is given by a combination of the four sources of error

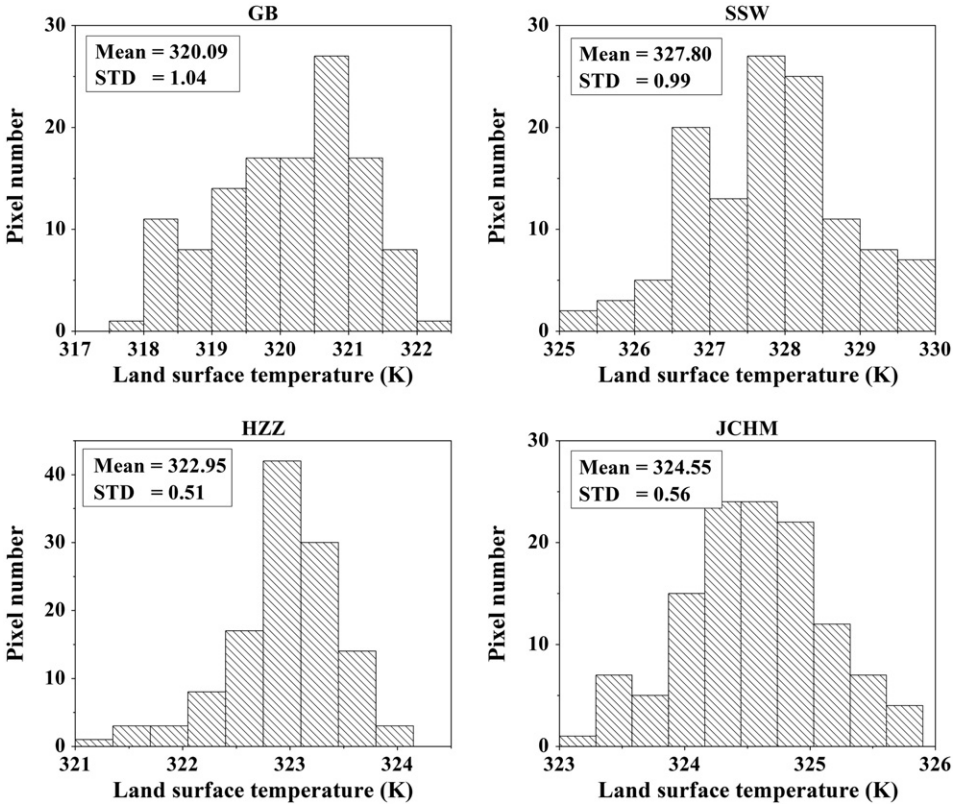

Fig. 2. Histograms of land surface temperature for the 11 × 11 ASTER pixels at four sites on August 27, 2012.

Table 3
Summary of evaluation results for the VIIRS LST product at four sites.

Site	Day				Night			
	Bias	STD	RMSE	N	Bias	STD	RMSE	N
GB	1.68	2.04	2.61	28	−0.70	0.58	0.90	27
SSW	−0.08	2.17	2.14	36	−2.26	1.53	2.72	36
HZZ	1.76	3.09	3.52	37	0.65	1.09	1.26	39
JCHM	−1.92	1.92	2.70	80	−0.01	1.02	1.02	93
All	0.36	2.31	2.74	181	−0.58	1.06	1.48	195

(calibration, emissivity correction, temporal and spatial uncertainty) (Niclòs et al., 2011), as follows:

$$\delta(T_s) = \left[\delta(\text{cal})^2 + \delta(\text{emis})^2 + \delta(\text{temp})^2 + \delta(\text{spat})^2\right]^{1/2}. \quad (8)$$

Values of 1.65 K, 1.72 K, 0.90 K and 0.75 K were obtained for the GB, SSW, HZZ and JCHM sites, respectively. It can be observed that the JCHM site shows the smallest LST uncertainties at daytime, and the uncertainties should be smaller at nighttime for all sites.

3.6. VIIRS and MODIS products

The VIIRS and Terra/Aqua MODIS products were acquired over the evaluation sites for all cases listed in Table 1. For VIIRS, the LST EDR and corresponding moderate-bands terrain corrected geolocation Sensor Data Records (SDR) (GMTCO) at 750 m resolution were used. For MODIS, the collection 5 LST products MOD11_L2 (Terra) and MYD11_L2 (Aqua) at 1 km resolution and the corresponding M*D03 geolocation products were used. The M*D is used for both the Terra (MOD) and Aqua (MYD) products.

Based on the geo-location information (latitude and longitude) of each evaluation site, the LST values of the VIIRS and MODIS products were extracted for the pixel closest to the evaluation site. Additionally, the satellite overpass time, sensor view zenith angle, MODIS band 31/32 emissivity, quality flag (QF) of VIIRS and quality control (QC) of MODIS were also extracted. According to the QF or QC information, only high/good quality data of VIIRS/MODIS LST products were used for evaluation. Next, the VIIRS and MODIS LSTs were matched with the ground-measured LSTs according to the satellite observation time. The satellite observation time was derived by linearly interpolating the start and end times of each VIIRS and MODIS product swath. In addition, all valid points were also examined manually to exclude cloud contaminated pixels with unreasonably low LST values.

4. Results

4.1. VIIRS LST

The VIIRS LSTs and MODIS LSTs were compared with the ground-measured LSTs, and the cases with differences larger than 10 K were treated as outliers and excluded for statistics. The results of comparisons

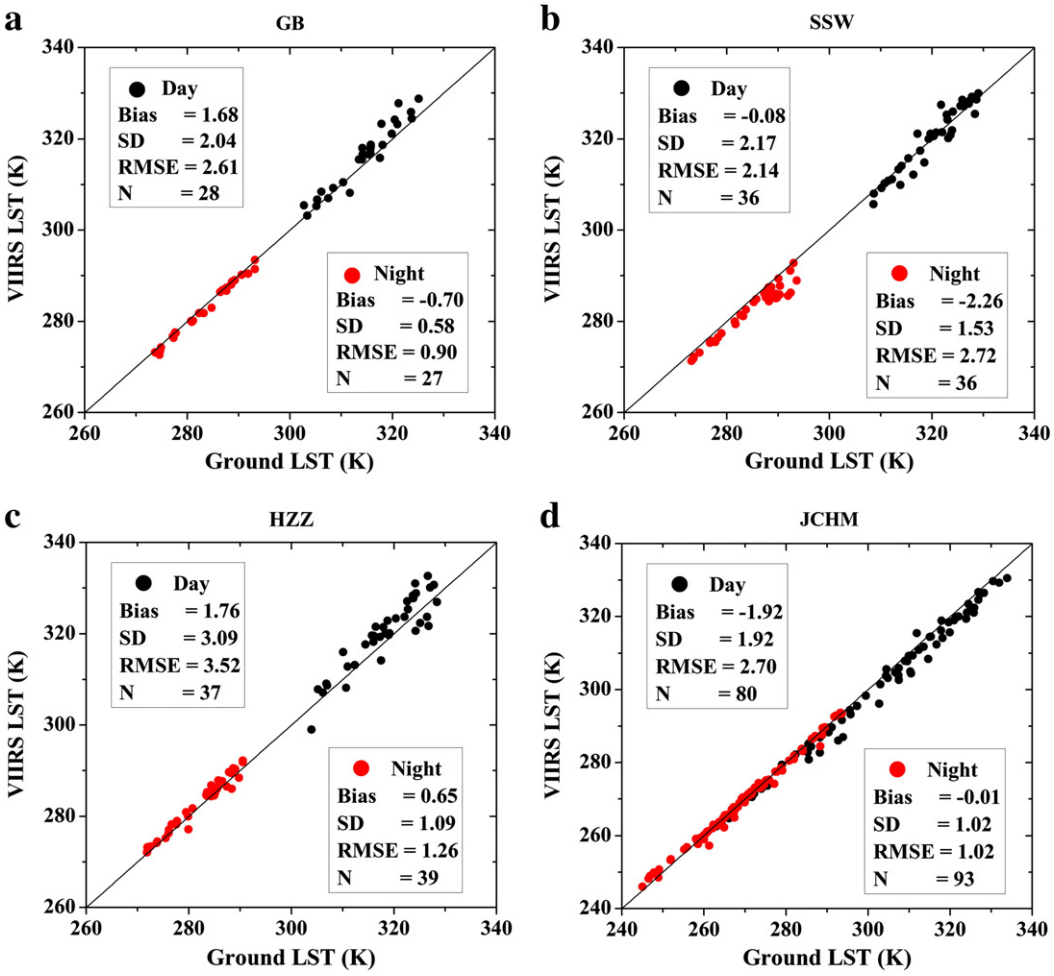

Fig. 3. Scatterplots between the VIIRS LST and ground LST for (black) daytime and (red) nighttime at the four sites.

between VIIRS LST and the ground LST are summarized in Table 3. Fig. 3 shows scatterplots of the VIIRS LST and ground LST for day and night observations at the four evaluation sites.

For the four sites at daytime, the VIIRS bias varies from −1.92 K to 1.76 K, with an average of 0.36 K; the STD varies from 1.92 K to 3.09 K, with an average of 2.31 K; and the root mean square error (RMSE) varies from 2.14 K to 3.52 K, with an average of 2.74 K. The VIIRS LSTs are warmer than the ground LSTs for the GB and HZZ sites and colder than the ground LSTs for the JCHM site during daytime. Although the HZZ and JCHM sites have similar land cover types, the LST biases showed contrast.

For the four sites at nighttime, the bias varies from −2.26 K to 0.65 K, with an average of −0.58 K; the STD varies from 0.58 K to 1.53 K, with an average of 1.06 K; and the RMSE varies from 0.90 K to 2.72 K, with an average of 1.48 K. The evaluation results for nighttime are better than those during daytime, especially in terms of RMSE. The daytime RMSEs are greater than 2 K for all four sites, and the nighttime RMSEs are much smaller, approximately 1 K for all sites except the SSW site. This is because the atmospheric water vapor is less and the land surface behaves almost homogeneously at night. Therefore, the ground temperature measurements during nighttime are more representative of the LST at the satellite pixel scale than those during daytime. This was consistent with the results of other studies (Guillevic et al., 2012; Hulley & Hook, 2012; Wang & Liang, 2009; Yu et al., 2005). The cold bias (−2.26 K) for the SSW site indicates that the VIIRS LST algorithm underestimates the LST for the sand surfaces at nighttime.

The VIIRS LST products were generated with two algorithms. Prior to August 10, 2012, the DSW algorithm was performed as the baseline algorithm for LST production. After August 10, 2012, the SW algorithm was executed as the baseline algorithm for LST production. The accuracies of these two algorithms were compared and the results of the comparison between the DSW and SW algorithms for daytime and nighttime at four sites are summarized in Table 4 and Table 5, respectively.

For the daytime results, the RMSEs for the DSW algorithm were larger than those of the SW algorithm at all four sites, with averages of 3.38 K and 2.36 K, respectively. This result indicates that the SW algorithm provides better performance than the DSW algorithm at daytime, consistent with the results of Yu et al. (2005).

For the nighttime results, the two algorithms obtain similar results except for the SSW site, with an average of 1.70 K and 1.16 K for the RMSE results, respectively. For the SSW site, the nighttime DSW algorithm underestimates the LST by 3 K, whereas the SW algorithm provides much better results with an RMSE of 1.64 K. This means that the SW algorithm can provide more stable results for different land surface types at nighttime.

4.2. MODIS LST

Figs. 4 and 5 show the scatterplots of the MODIS LST and ground LST, respectively, for Terra and Aqua observations at the four sites. The comparison results for the Terra and Aqua MODIS LST products are summarized in Table 6 and Table 7, respectively.

The daytime biases in the Terra MODIS LST are negative for the four sites, indicating an underestimation of the LST for the barren surface types, and the JCHM showed the largest bias (−3.13 K). The nighttime biases were much smaller for all sites except for the SSW site. The large cold bias (−2.66 K) for the SSW site indicates that the MODIS LST algorithm underestimates the LST for sand surfaces at nighttime, similar to the VIIRS LST algorithm. The daytime LST RMSEs were lowest for the GB site (1.73 K) and increased substantially for the HZZ (2.73 K), SSW (2.75 K) and JCHM (3.83 K) sites. The nighttime RMSEs are smaller in magnitude than the daytime RMSEs except for the SSW sites.

The daytime Aqua MODIS LST results are similar to the Terra MODIS LST results at the four sites, but the biases and RMSEs are much larger, with three sites (GB, HZZ, JCHM) showing biases and RMSEs greater than 3 K. These results indicate that both the Terra and Aqua MODIS C5 LST products underestimate the LST for barren surfaces at daytime, consistent with the results of Wan (2014). Wan (2014) indicates that there are two possible reasons for the large LST errors at barren surface sites. First, the original split-window algorithm does not well cover the wide range of LSTs, namely, the daytime LSTs are greater than the air temperature at the surface level by more than 16 K, which is beyond the upper limit ($T_{s\text{-air}}$ + 16 K) used in the current MODIS C5 LST products algorithm development (Wan, 2014; Wan & Li, 2008). Second, the large errors in surface emissivity values in MODIS bands 31 and 32 estimated from land cover types.

The daytime differences between the ground measured LSTs and the 5 m air temperatures for the three barren surface sites are summarized in Table 8. It can be observed that the differences are both greater than 16 K for the Terra and Aqua observations, with average biases of 19.07 K and 20.26 K, respectively. In order to solve this problem, two separate sets of coefficients developed for the type of bare soil in the hot and warm bare soil regions based on simulation of a much wider LST range have been used in the refined version of the GSW algorithm to produce the collection 6 MODIS LST product, and the validation results indicate that the refined GSW algorithm works well in both daytime and nighttime cases at most bare soils sites (Wan, 2014).

In order to investigate whether the large negative biases were also caused by inaccurate emissivity values in MODIS bands 31 and 32, the land surface emissivity (LSE) values in ASTER band 14 (11.3 μm) were used for comparison with MODIS band 31 (11.03 μm) emissivity values. Numerical simulations by Gillespie et al. (1998) indicated that ASTER TES algorithm should be able to recover emissivities within about ± 0.015 for all bands, but Hulley, Hughes, and Hook (2012) indicated that ASTER band 14 emissivity uncertainty retrieved by TES algorithm is approximately below 0.005 over bare surface (rocks, soils, sand). The ASTER band 14 LSEs for the 11 × 11 pixels (1 km^2) centered on the evaluation site were extracted, and the average values and STDs were calculated for the twelve scenes. LSE values in MODIS bands 31 and 32 and ASTER band 14 for the four sites are summarized in Table 9. It can be found that the LSE values in MODIS band 31 are overestimated by approximately 0.007 for GB and SSW sites when compared with the LSE values in ASTER band 14, which would result in an underestimation of LST. The split-window algorithm is very sensitive to emissivity errors, and the sensitivity is significantly higher for direr atmospheres, a 0.005 error in emissivity will result in a LST error of 1 K or more under drier conditions (Freitas, Trigo, Bioucas-Dias, &

Table 4
Summary of daytime evaluation results for the VIIRS DSW and SW algorithms at four sites.

Site	Daytime DSW				SW			
	Bias	STD	RMSE	N	Bias	STD	RMSE	N
GB	1.82	3.78	3.90	6	1.64	1.39	2.13	22
SSW	−0.26	2.71	2.63	16	0.06	1.68	1.63	20
HZZ	1.36	4.08	4.17	15	2.03	2.27	3.00	22
JCHM	−1.54	2.54	2.83	8	−1.96	1.85	2.69	72
All	0.35	3.28	3.38	45	0.44	1.80	2.36	136

Table 5
Summary of nighttime evaluation results for the VIIRS DSW and SW algorithms at four sites.

Site	Nighttime DSW				SW			
	Bias	STD	RMSE	N	Bias	STD	RMSE	N
GB	−0.73	0.72	0.99	6	−0.69	0.56	0.88	21
SSW	−3.24	1.93	3.73	15	−1.56	0.52	1.64	21
HZZ	0.87	1.23	1.48	17	0.49	0.96	1.06	22
JCHM	0.23	0.61	0.61	8	−0.04	1.05	1.05	85
All	−0.72	1.12	1.70	46	−0.45	0.77	1.16	149

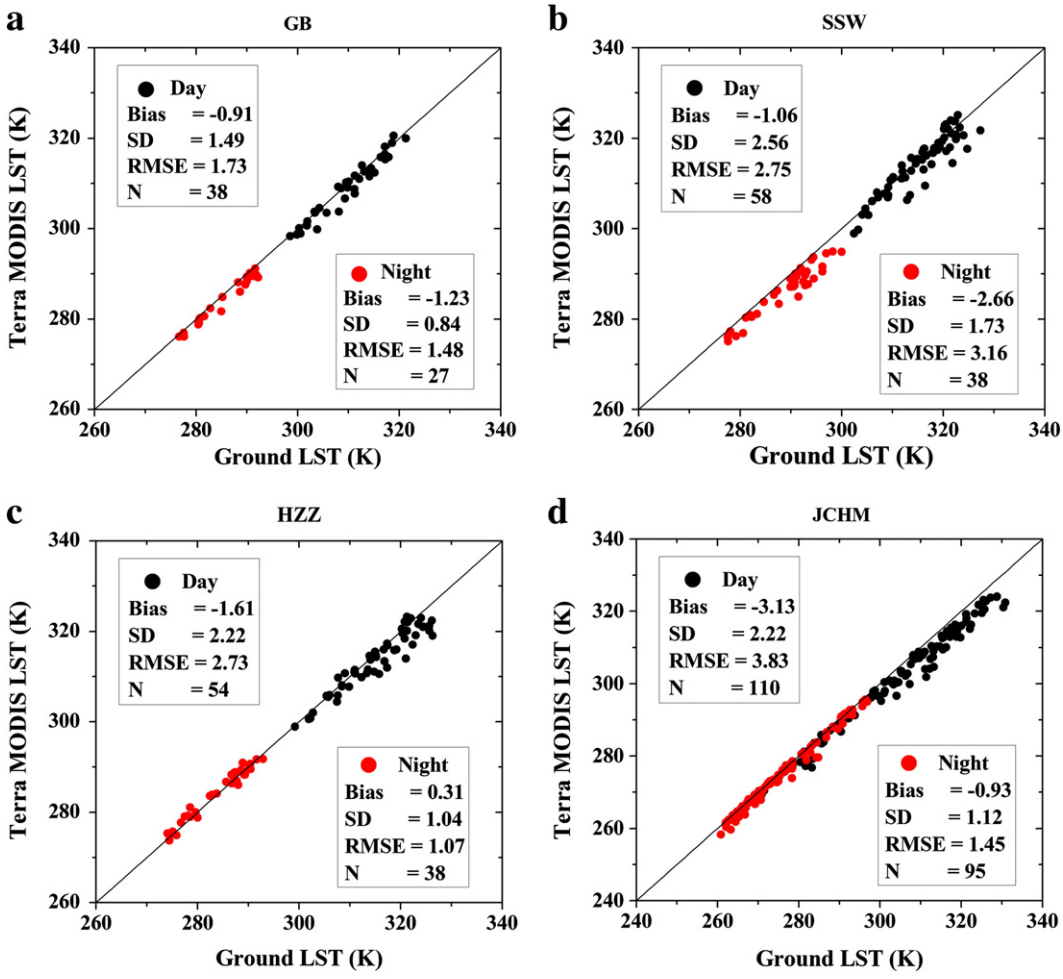

Fig. 4. Scatterplots between the Terra MODIS LST and ground LST for (black) daytime and (red) nighttime at the four sites.

Göttsche, 2010; Galve, Coll, Caselles, & Valor, 2008; Yu et al., 2008). This is more evident for the nighttime evaluation results for GB and SSW sites which both have large negative biases for Terra and Aqua products, because the difference in LST and air temperature does not play a role at nighttime. The LSE values in MODIS band 31 and ASTER band 14 are very close for the HZZ and JCHM sites, thus the nighttime Aqua MODIS LST results are much better for these two sites, with all biases smaller than 1 K and RMSEs smaller than 1.6 K. Hulley, Hook, and Hughes (2012) also pointed out that the MOD11 LST products underestimated LST by 3–4 K at five pseudo-invariant sand dune sites in the southwestern United States due to an overestimation of the emissivity values for sand dune. In order to solve this problem, Wan (2014) proposed a prototype emissivity adjustment model for bare soil pixels, and the preliminary results indicated that the emissivity adjustment model was useful to reduce the MODIS collection 6 LST product error. It should be noted that the daytime biases in VIIRS and MODIS LST at SSW site are smaller than those of nighttime. The possible reason for this is that there are relatively large spatial variations in LST at SSW site than other three sites at daytime (Fig. 2 and Table 2), which will cancel out some of the errors caused by inaccurate emissivity estimation.

In general, the VIIRS LST products provide better accuracy both for daytime and nighttime conditions compared with the Aqua MODIS C5 LST products, which have the close overpass time. There are two possible reasons for such results. First, the spatial resolution of the VIIRS LST product is greater than that of MODIS LST product. Second, only the VIIRS LSTs with a satellite view zenith angle (VZA) less than 40° were used for evaluation, considering that the VIIRS high-quality LST product only contains LSTs with a VZA less than 40°. The errors in the LST product are generally larger for an LST with a larger VZA. The comparison results for the Terra and Aqua MODIS LSTs with a VAZ less that 40° are also summarized in Table 10 and Table 11, respectively. The accuracy of both the Terra and Aqua MODIS LSTs are improved at daytime when compared with the results for all values of VZA, and the average RMSE was improved from 2.76 K to 1.90 K for Terra and from 3.80 K to 2.70 K for Aqua. Nevertheless, the accuracy at nighttime is not significantly improved.

5. Discussion and conclusions

LST is a key variable for hydrological, meteorological, climatological and environmental studies. Many remote sensing LST products have been generated in the past, but quantifying the accuracy of different LST products will both improve their utility and help refine the LST retrieval algorithms. The study reported in this paper evaluated the accuracy of two LST products: the VIIRS LST EDR and MODIS collection 5 L2 LST products from the Terra and Aqua satellites. Conventional T-based method was performed using ground LST measurements collected from four barren surface sites in an arid area of northwest China during the HiWATER experiment which took place from June 2012 to April 2013. Two types of ground measurements were used to obtain the ground LSTs. The first type is the surface longwave radiation measured by the CNR 1 net radiometer, and the second is the radiometric ground

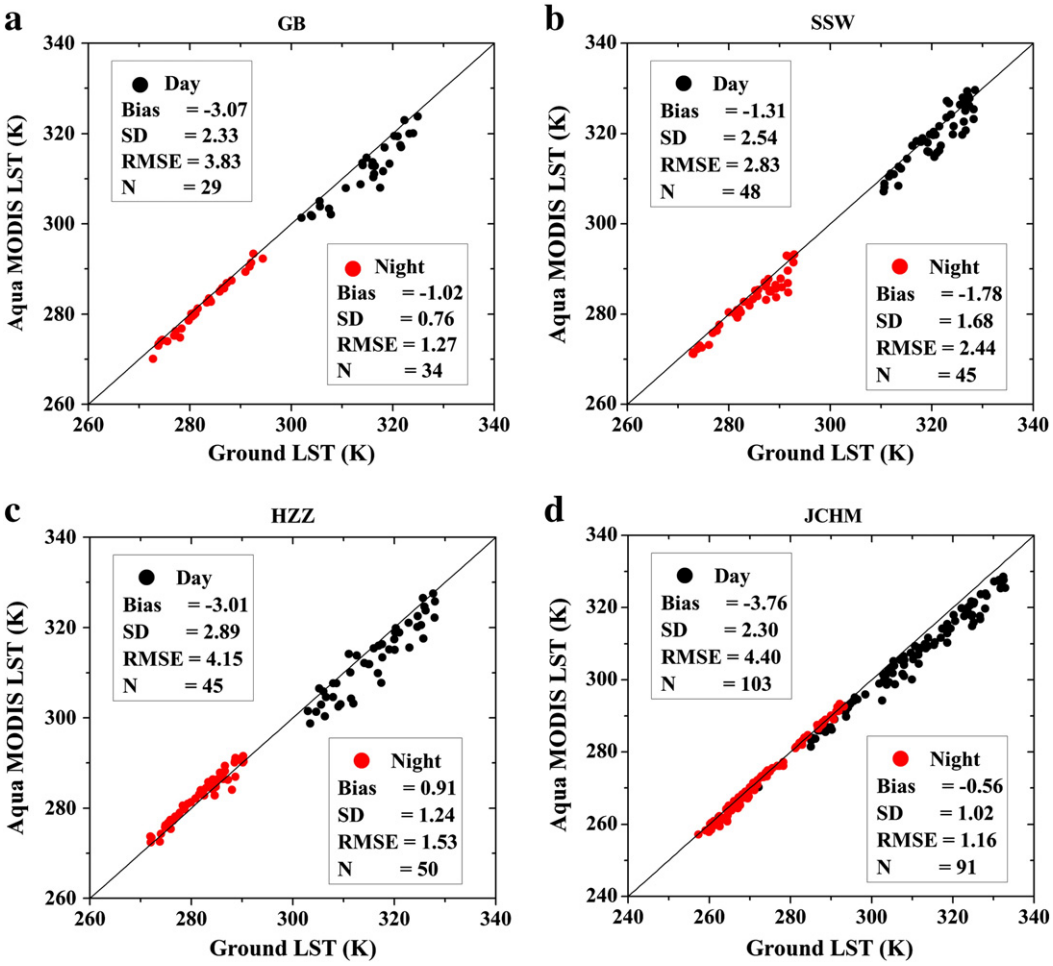

Fig. 5. Scatterplots between the Aqua MODIS LST and ground LST for (black) daytime and (red) nighttime at the four sites.

surface temperature measured by the SI-111 radiometer. Both ground measurements were transferred to the ground LSTs and directly compared with the satellite LSTs at the pixel scale.

The results indicate that the current VIIRS LST products yield a reasonable accuracy, with average biases of 0.36 K and −0.58 K and average RMSEs of 2.74 K and 1.48 K for the four sites at daytime and nighttime, respectively. However, three barren sites at daytime and one barren surface site at nighttime showed absolute biases larger than 1.5 K. Additionally, the accuracy for nighttime is much better than that of daytime. The daytime RMSEs are larger than 2 K for all four sites and the nighttime RMSEs are much smaller, near 1 K for all sites except for a sandy dune site (SSW), which indicates that the VIIRS LST products underestimate the LST for sand surfaces at nighttime. Furthermore, we also found that the SW algorithm can provide superior performance to that of DSW algorithm at both daytime and nighttime.

For MODIS, the results indicate that the Terra and Aqua MODIS C5 LST products underestimate the LST for the four barren surface sites at daytime, and the biases and RMSEs are much larger for Aqua, with biases ranging from −0.91 K to −3.13 K for Terra and from −1.31 K to −3.76 K for Aqua. There are two reasons for the large LST errors at barren surface sites. First, the daytime LSTs are larger than the air temperature at the surface level by more than 16 K which is beyond the upper limit ($T_{s\text{-air}}$ + 16 K) used in the current MODIS C5 LST products algorithm development. Second, it is due to the large errors in surface emissivity values in MODIS bands 31 and 32 estimated from land cover types. Thus, in order to solve these problems, two separate sets of coefficients developed for the type of bare soil in the hot and warm bare soil regions based on a much wider LST range simulation and a emissivity adjustment model have been used in the new version of the GSW algorithm to improve the collection 6 MODIS LST product (Wan, 2014).

As pointed out by Wan (2008), it is very difficult to validate LST at 1 km or larger pixel scale. Because of the large spatial variation in LSTs, especially during the daytime, it is very difficult to find suitable

Table 6
Summary of evaluation results for the Terra MODIS LST product at four sites.

Site	Day				Night			
	Bias	STD	RMSE	N	Bias	STD	RMSE	N
GB	−0.91	1.49	1.73	38	−1.23	0.84	1.48	27
SSW	−1.06	2.56	2.75	58	−2.66	1.73	3.16	38
HZZ	−1.61	2.22	2.73	54	0.31	1.04	1.07	38
JCHM	−3.13	2.22	3.83	110	−0.93	1.12	1.45	95
All	−1.68	2.12	2.76	260	−1.13	1.18	1.79	198

Table 7
Summary of evaluation results for the Aqua MODIS LST product at four sites.

Site	Day				Night			
	Bias	STD	RMSE	N	Bias	STD	RMSE	N
GB	−3.07	2.33	3.83	29	−1.02	0.76	1.27	34
SSW	−1.31	2.54	2.83	48	−1.78	1.68	2.44	45
HZZ	−3.01	2.89	4.15	45	0.91	1.24	1.53	50
JCHM	−3.76	2.30	4.40	103	−0.56	1.02	1.16	91
All	−2.79	2.52	3.80	225	−0.61	1.18	1.60	220

Table 8
Daytime difference statistics between the ground-measured LST and air temperature.

Site	Terra		Aqua	
	Bias	STD	Bias	STD
GB	16.52	2.75	17.99	2.65
SSW	20.18	3.31	22.23	2.56
HZZ	20.50	3.85	20.55	4.17
All	19.07	3.30	20.26	3.13

homogeneous validation sites. Thus, large homogeneous lakes and croplands are ideal sites for LST validation (Coll et al., 2005; Wan et al., 2002). However, it is still very necessary to quantify the accuracy of different LST products at different surface types, such as the barren surface types in this study. There are also some shortcomings of this study which should be acknowledged. First, two sites (GB and SSW) used in this study have relatively large variations in LSTs, with uncertainty close to 1 K. Wan (2008) has indicated that ideal homogeneous validation site should have an uncertainty well below 1 K. Thus, the large variations in LSTs have an impact on the evaluation results, especially for the daytime results at SSW site. Second, we only used one point LST measurement for each site, which may not enough for validation of the LST at spatial resolution around or larger than 1 km for the barren surface. Thus, TIR radiometers with high accuracy should be used at multiple points in the same time to evaluate the spatial variations in barren surface in-situ LSTs. For most of the LST validation field campaigns in the past, the in-situ LSTs were measured manually by TIR radiometers at multiple points. However, this method is not suitable for the long-term LST validation due to the large cost of field campaigns and high temporal resolutions of current TIR sensors, such as MODIS and VIIRS. Recently, the power of wireless sensor network (WSN) technology has provided the capability of developing automatic, intelligent and remote-controllable large-scale systems for remote sensing algorithm and product validation (Jin et al., 2012; Li, Cheng, et al., 2013; Raissouni et al., 2013). It provides a new solution to perform long-term validation of multiple LST products at different scales in the future. Currently we have already established a WSN composed of six nodes which were designed to validate different kinds of remote sensing products at 1 km scale in a cropland area in Hebei province, China. The field observations include soil moisture, soil temperature, LST, leaf area index (LAI) and other ordinary meteorological parameters. Additionally, note that the results presented in this paper refer to arid areas with mid-latitude atmospheric conditions, and further evaluation is required for additional areas and atmospheric conditions.

Acknowledgments

The authors thank three anonymous reviewers for their helpful comments and suggestions that have significantly improved this article. This work was supported by NOAA JPSS program (NA12NES4400010), National High-Technology Research and Development Program of China (863 Project: 2012AA12A304), Chinese Natural Science Foundation Project (41101325, 91125003, 41271345), Chinese Academy of Sciences Action Plan for West Development Project (KZCX2-XB3-15), NOAA PSDI program (NA11NES4400012) and Chinese Academy of Sciences/State Administration of Foreign Experts Affairs (CAS/SAFEA) International Partnership Program (KZZD-EW-TZ-09). The ground data used in this study are obtained from the HiWATER experiment, we thank all the scientists, engineers, and students who participated in HiWATER field campaigns. This work is a part of the evaluation efforts for the VIIRS LST EDR public release and is supported by the VIIRS LST EDR team at the National Oceanic and Atmospheric Administration. The manuscript contents are solely the opinions of the authors and do not constitute a statement of policy, decision, or position on behalf of NOAA or the U.S. Government.

Table 9
Emissivity values in MODIS bands 31 and 32, and average emissivity values for 11 × 11 pixels in ASTER band 14 at four sites.

Site	MODIS ε_{31} (11.03 μm)	MODIS ε_{32} (12.02 μm)	ASTER ε_{14} (11.3 μm)
GB	0.972	0.976	0.965 ± 0.002
SSW	0.966	0.972	0.958 ± 0.001
HZZ	0.974 ± 0.002	0.980 ± 0.002	0.973 ± 0.003
JCHM	0.970 ± 0.001	0.975 ± 0.001	0.973 ± 0.002

Table 10
Summary of the evaluation results for the Terra MODIS LST results with a view zenith angle less than 40° at four sites.

Site	Day				Night			
	Bias	STD	RMSE	N	Bias	STD	RMSE	N
GB	−0.27	1.05	1.06	28	−0.86	0.49	0.98	17
SSW	0.05	1.79	1.77	40	−1.97	1.34	2.37	25
HZZ	−0.85	1.71	1.89	36	0.81	0.86	1.17	22
JCHM	−2.4	1.57	2.86	75	−0.58	0.93	1.09	53
All	−0.87	1.53	1.90	179	−0.65	0.91	1.40	117

Table 11
Summary of the evaluation results for the Aqua MODIS LST results with a view zenith angle less than 40° at four sites.

Site	Day				Night			
	Bias	STD	RMSE	N	Bias	STD	RMSE	N
GB	−1.95	1.36	2.35	12	−0.88	0.91	1.25	18
SSW	−0.01	1.87	1.84	27	−1.41	1.67	2.16	29
HZZ	−1.83	2.57	3.11	26	0.97	1.11	1.46	31
JCHM	−2.97	1.87	3.51	65	−0.44	0.97	1.06	52
All	−1.69	1.92	2.70	130	−0.44	1.17	1.48	130

References

Anderson, M. C., Kustas, W. P., Norman, J. M., Hain, C. R., Mecikalski, J. R., Schultz, L., et al. (2011). Mapping daily evapotranspiration at field to continental scales using geostationary and polar orbiting satellite imagery. *Hydrology and Earth System Sciences*, *15*, 223–239, http://dx.doi.org/10.5194/hess-15-223-2011.

Anderson, M. C., Norman, J. M., Diak, G. R., Kustas, W. P., & Mecikalski, J. R. (1997). A two-source time-integrated model for estimating surface fluxes using thermal infrared remote sensing. *Remote Sensing of Environment*, *60*, 195–216.

Baldridge, A.M., Hook, S. J., Grove, C. I., & Rivera, G. (2009). The ASTER spectral library version 2.0. *Remote Sensing of Environment*, *113*, 711–715.

Borel, C. (1998). Surface emissivity and temperature retrieval for a hyperspectral sensor. *Proceedings of the 1998 IEEE International Geoscience and Remote Sensing Symposium, Seattle, USA* (pp. 546–549).

Cheng, J., Liang, S., Yao, Y., & Zhang, X. (2013). Estimating the optimal broadband emissivity spectral range for calculating surface longwave net radiation. *IEEE Geoscience and Remote Sensing Letters*, *10*, 401–405.

Coll, C., Caselles, V., Galve, J. M., Valor, E., Niclòs, R., Sánchez, J. M., et al. (2005). Ground measurements for the validation of land surface temperatures derived from AATSR and MODIS data. *Remote Sensing of Environment*, *97*, 288–300.

Coll, C., Caselles, V., Valor, E., Niclòs, R., Sánchez, J. M., Galve, J. M., et al. (2007). Temperature and emissivity separation from ASTER data for low spectral contrast surfaces. *Remote Sensing of Environment*, *110*, 162–175.

Coll, C., Valor, E., Galve, J. M., Mira, M., Bisquert, M., García-Santos, V., et al. (2012). Long-term accuracy assessment of land surface temperatures derived from the Advanced Along-Track Scanning Radiometer. *Remote Sensing of Environment*, *116*, 211–225.

Coll, C., Wan, Z., & Galve, J. M. (2009). Temperature-based and radiance-based validations of the V5 MODIS land surface temperature product. *Journal of Geophysical Research*, *114*, D20102, http://dx.doi.org/10.1029/2009JD012038.

Freitas, S.C., Trigo, I. F., Bioucas-Dias, J. M., & Göttsche, F. M. (2010). Quantifying the uncertainty of land surface temperature retrievals from SEVIRI/Meteosat. *IEEE Transactions on Geoscience and Remote Sensing*, *48*, 523–534.

Galve, J. M., Coll, C., Caselles, V., & Valor, E. (2008). An atmospheric radiosounding database for generating land surface temperature algorithms. *IEEE Transactions on Geoscience and Remote Sensing*, *46*, 1547–1557.

Gillespie, A.R., Rokugawa, S., Matsunaga, T., Cothern, J. S., Hook, S., & Kahle, A.B. (1998). A temperature and emissivity separation algorithm for Advanced Spaceborne Thermal Emission and Reflection Radiometer (ASTER) images. *IEEE Transactions on Geoscience and Remote Sensing*, *36*, 1113–1126.

Gui, D., Zeng, F., Liu, Z., & Zhang, B. (2013). Root characteristics of *Alhagi sparsifolia* seedlings in response to water supplement in an arid region, northwestern China. *Journal of Arid Land*, *5*, 542–551.

Guillevic, P. C., Privette, J. L., Coudert, B., Palecki, M.A., Demarty, J., Ottlé, C., et al. (2012). Land surface temperature product validation using NOAA's surface climate

observation networks-scaling methodology for the Visible Infrared Imager Radiometer Suite (VIIRS). *Remote Sensing of Environment*, *124*, 282–298.
Hook, S. J., Vaughan, R. G., Tonooka, H., & Schladow, S. G. (2007). Absolute radiometric in-flight validation of mid infrared and thermal infrared data from ASTER and MODIS on the Terra spacecraft using the Lake Tahoe, CA/NV, USA, Automated Validation Site. *IEEE Transactions on Geoscience and Remote Sensing*, *45*, 1798–1807.
Hulley, G. C., & Hook, S. J. (2012). A radiance-based method for estimating uncertainties in the Atmospheric Infrared Sounder (AIRS) land surface temperature product. *Journal of Geophysical Research*, *117*, D20117, http://dx.doi.org/10.1029/2012JD018102.
Hulley, G. C., Hook, S. J., & Hughes, T. (2012). *MODIS MOD21 land surface temperature and emissivity algorithm theoretical basis document. JPL Publication 12-17*: Jet Propulsion Laboratory, California Institute of Technology.
Hulley, G. C., Hughes, T., & Hook, S. J. (2012). Quantifying uncertainties in land surface temperature (LST) and emissivity retrievals from ASTER and MODIS thermal infrared data. *Journal of Geophysical Research*, *117*, D23113, http://dx.doi.org/10.1029/2012JD018506.
Ingram, P.M., & Muse, A. H. (2001). Sensitivity of iterative spectrally smooth temperature/emissivity separation to algorithmic assumptions and measurement noise. *IEEE Transactions on Geoscience and Remote Sensing*, *39*, 2158–2167.
Jiménez-Muñoz, J. C., & Sobrino, J. A. (2003). A generalized single-channel method for retrieving land surface temperature from remote sensing data. *Journal of Geophysical Research*, *108*, 4688–4695.
Jin, R., Li, X., Yan, B., Luo, W., Li, X., Guo, J., et al. (2012). Introduction of eco-hydrological wireless sensor network in the Heihe River Basin. *Advances in Earth Sciences*, *27*, 993–1005 (in Chinese).
Li, X., Cheng, G., Liu, S., Xiao, Q., Ma, M., Jin, R., et al. (2013). Heihe watershed allied telemetry experimental research (HiWATER): Scientific objectives and experimental design. *Bulletin of the American Meteorological Society*, *94*, 1145–1160.
Li, H., Liu, Q., Du, Y., Jiang, J., & Wang, H. (2013). Evaluation of the NCEP and MODIS atmospheric products for single channel land surface temperature retrieval with ground measurements: A case study of HJ-1B IRS data. *IEEE Journal of Selected Topics in Applied Earth Observations and Remote Sensing*, *6*, 1399–1408.
Li, H., Liu, Q., Zhong, B., Du, Y., Wang, H., & Wang, Q. (2010). A single-channel algorithm for land surface temperature retrieval from HJ-1B/IRS data based on a parametric model. *IEEE International Geoscience and Remote Sensing Symposium, Honolulu, USA* (pp. 2448–2451).
Li, Z. -L., Tang, B. -H., Wu, H., Ren, H., Yan, G., Wan, Z., et al. (2013). Satellite-derived land surface temperature: Current status and perspectives. *Remote Sensing of Environment*, *131*, 14–37.
Li, H., Wang, H., Du, Y., Liu, Q., Sun, D., Yu, Y., et al. (in preparation). *Validation of the land surface temperature and emissivity derived from ASTER data in the HiWATER experiment.*
Liu, Y., Mu, X., Wang, H., & Yan, G. (2011). A novel method for extracting green fractional vegetation cover from digital images. *Journal of Vegetation Science*, *23*, 406–418.
Liu, S., Li, X., Xu, Z., Xiao, Q., Ma, M., Jin, R., et al. (in preparation). *The multi-scale observation experiment on evapotranspiration over heterogeneous land surfaces (HiWATER-MUSOEXE): Flux Observation Matrix.*
Niclòs, R., Galve, J. M., Valiente, J. A., Estrela, M. J., & Coll, C. (2011). Accuracy assessment of land surface temperature retrievals from MSG2-SEVIRI data. *Remote Sensing of Environment*, *115*, 2126–2140.
Pinheiro, A.C., Descloitres, J., Privette, J. L., Susskind, J., Iredell, L., & Schmaltz, J. (2007). Near-real time retrievals of land surface temperature within the MODIS rapid response system. *Remote Sensing of Environment*, *106*, 326–336.
Qin, Z., Karnieli, A., & Berliner, P. (2001). A mono-window algorithm for retrieving land surface temperature from Landsat TM data and its application to the Israel–Egypt border region. *International Journal of Remote Sensing*, *22*, 3719–3746.
Raissouni, N., Sobrino, J. A., Chahboun, N. Ben, Achhab, A., Lahraoua, M., & Azyat, A. (2013). First results towards building up a reliable in situ measurements database for LST algorithm validations using modular WSN: Northern Morocco campaigns case study. *International Journal of Remote Sensing*, *34*, 3153–3163.
Rajasekar, U., & Weng, Q. (2009). Urban heat island monitoring and analysis by data mining of MODIS imageries. *ISPRS Journal of Photogrammetry and Remote Sensing*, *64*, 86–96.
Sun, D., Ji, Y., Ardanuy, P., Keally, P., & Yang, W. (2000). *NOPESS VIIRS land surface temperature algorithm theoretical basis document version 1-4.*
Sun, D., & Pinker, R. T. (2003). Estimation of land surface temperature from a Geostationary Operational Environmental Satellite (GOES-8). *Journal of Geophysical Research*, *108*, 4326, http://dx.doi.org/10.1029/2002JD002422 (D11).
Sun, D., Yu, Y., Fang, L., & Liu, Y. (2013). Toward an operational land surface temperature algorithm for GOES. *Journal of Applied Meteorology and Climatology*, *52*, 1974–1986.
Tonooka, H. (2005). Accurate atmospheric correction of ASTER thermal infrared imagery using the WVS method. *IEEE Transactions on Geoscience and Remote Sensing*, *43*, 2778–2792.
Valor, E., & Caselles, V. (1996). Mapping land surface emissivity from NDVI: Application to European, African, and South American areas. *Remote Sensing of Environment*, *57*, 167–184.
Vancutsem, C., Ceccato, P., Dinku, T., & Connor, S. (2010). Evaluation of MODIS land surface temperature data to estimate air temperature in different ecosystems over Africa. *Remote Sensing of Environment*, *114*, 449–465.
Wan, Z. (2008). New refinements and validation of the MODIS land-surface temperature/emissivity products. *Remote Sensing of Environment*, *112*, 59–74.
Wan, Z. (2014). New refinements and validation of the collection-6 MODIS land-surface temperature/emissivity product. *Remote Sensing of Environment*, *140*, 36–45.
Wan, Z., & Dozier, J. (1996). A generalized split-window algorithm for retrieving land-surface temperature from space. *IEEE Transactions on Geoscience and Remote Sensing*, *34*, 892–905.
Wan, Z., & Li, Z. -L. (1997). A physics-based algorithm for retrieving land-surface emissivity and temperature from EOS/MODIS data. *IEEE Transactions on Geoscience and Remote Sensing*, *35*, 980–996.
Wan, Z., & Li, Z. -L. (2008). Radiance-based validation of the V5 MODIS land-surface temperature product. *International Journal of Remote Sensing*, *29*, 5373–5395.
Wan, Z., Zhang, Y., Zhang, Q., & Li, Z. -L. (2002). Validation of the land-surface temperature products retrieved from Terra Moderate Resolution Imaging Spectroradiometer data. *Remote Sensing of Environment*, *83*, 163–180.
Wang, K., & Liang, S. (2009). Evaluation of ASTER and MODIS land surface temperature and emissivity products using long-term surface longwave radiation observations at SURFRAD sites. *Remote Sensing of Environment*, *113*, 1556–1565.
Wang, W., Liang, S., & Meyer, T. (2008). Validating MODIS land surface temperature products using long-term nighttime ground measurements. *Remote Sensing of Environment*, *112*, 623–635.
Wang, K., Wan, Z., Wang, P., Sparrow, M., Liu, J., & Haginoya, S. (2007). Evaluation and improvement of the MODIS land surface temperature/emissivity products using ground-based measurements at a semidesert site on the western Tibetan Plateau. *International Journal of Remote Sensing*, *28*, 2549–2565.
Weng, Q., Lu, D., & Schubring, J. (2004). Estimation of land surface temperature–vegetation abundance relationship for urban heat island studies. *Remote Sensing of Environment*, *89*, 467–483.
Xu, Z., Liu, S., Li, X., Shi, S., Wang, J., Zhu, Z., et al. (2013). Intercomparison of surface energy flux measurement systems used during the HiWATER-MUSOEXE. *Journal of Geophysical Research*, *118*, http://dx.doi.org/10.1002/2013JD020260.
Yu, Y., Privette, J. L., & Pinheiro, A.C. (2005). Analysis of the NPOESS VIIRS land surface temperature algorithm using MODIS data. *IEEE Transactions on Geoscience and Remote Sensing*, *43*, 2340–2350.
Yu, Y., Privette, J. L., & Pinheiro, A.C. (2008). Evaluation of split-window land surface temperature algorithms for generating climate data records. *IEEE Transactions on Geoscience and Remote Sensing*, *46*, 179–192.
Yu, Y., Tarpley, D., Privette, J. L., Flynn, L. E., Xu, H., Chen, M., et al. (2012). Validation of GOES-R satellite land surface temperature algorithm using SURFRAD ground measurements and statistical estimates of error properties. *IEEE Transactions on Geoscience and Remote Sensing*, *50*, 704–713.
Yu, Y., Tarpley, D., Privette, J. L., Goldberg, M.D., Rama Varma Raja, M. K., Vinnikov, K. Y., et al. (2009). Developing algorithm for operational GOES-R land surface temperature product. *IEEE Transactions on Geoscience and Remote Sensing*, *47*, 936–951.
Zhou, L., Dickinson, R. E., Tian, Y., Jin, M., Ogawa, K., Yu, H., et al. (2003). A sensitivity study of climate and energy balance simulations with use of satellite-derived emissivity data over northern Africa and the Arabian Peninsula. *Journal of Geophysical Research*, *108*(D24), 4795, http://dx.doi.org/10.1029/2003JD004083.